JOURNAL OF Materials CHEMISTRY

# Structure and nanomechanics of linear dendronised polymers: a molecular simulation study†

**Demetri K. Christopoulos,[a] Demetri J. Photinos,[a] Lorna M. Stimson,*[a] Andreas F. Terzis[b] and Alexandros G. Vanakaras[a]**

[a]*Department of Materials Science, University of Patras, Patras 26500, Greece. E-mail: stimson@upatras.gr*
[b]*Department of Physics, University of Patras, Patras 26500, Greece*

***Received 14th April 2003, Accepted 2nd June 2003***
***First published as an Advance Article on the web 24th September 2003***

We use Monte Carlo algorithms to simulate, on the atomistic scale, the structure and rigidity of model linear dendronised polymers (LDPs) consisting of a poly(*para*-phenylene) backbone with laterally substituted Fréchet type dendritic units. A coarse-grained representation of united atoms interacting *via* steric repulsions is employed for the study of the equilibrium structure of single LDPs as a function of dendron generation, $g$. Backbone conformation averages and dendron mass distributions are calculated for $g = 0$ to 5 and are used to elucidate the mechanism of stiffening of the LDP with increasing $g$. Congestion-induced stiffening, reflecting on the response of the backbone to linear extension as well as to bend and torsion deformations, is clearly detected for $g = 4$ and is dramatically intensified at $g = 5$ where, in addition, strongly bent and twisted structures develop along the backbone contour and reduce appreciably the equilibrium elongation of the LDP.

## 1. Introduction

Dendrimers are molecules of repetitive branching architecture. As a relatively new class of materials they have received a great deal of attention due to their unique physical, chemical and biological properties and the related broad range of potential applications.[1–3] More recently, the polymerisation of dendritic structures has produced the so-called dendronized polymers.[4,5] Commonly, these consist of a linear polymer chain (the backbone) with laterally substituted dendritic units (the dendra). The possibility of controlled shapes and dimensions on the nanoscale, together with the many combinations of repetitive units, functionalities, phobicities/philicities *etc.*, presented by dendronised polymers has opened up a new dimension in materials properties and potential applications.

The macromolecular structure of a linear dendronised polymer (LDP) is determined by the structures of the individual dendra and of the linear polymer backbone, by their interactions and by the dendron grafting density along the backbone contour. The generation, $g$, of the dendron is an essential parameter both for single dendrimers and for LDPs. For given branch size, $b$, and coordination number, $f$ (number of connected branches at each branching point), the spatial dimensions and the mass distribution of a single dendrimer are controlled by $g$. Depending on $b$ and $f$, the dendrimer generation may reach a finite terminal value $g_t = g_t(b,f)$ beyond which a packing catastrophe (overcongestion) takes place and the dendrimer cannot be formed. In LDPs, the generation of the dendra obviously controls the lateral dimension of the decorated backbone but it could also influence its internal motions, thereby controlling the effective rigidity and elongation of the entire LDP. Moreover, a second type of packing catastrophe could limit the generation of dendra in a LDP from exceeding a terminal value, $g_t^{LDP}$; the overcongestion in this case is caused by the lack of space to accommodate a dendron and its adjacent backbone segment or its nearest dendron neighbours. The latter situation occurs at sufficiently high grafting densities and naturally the terminal generation $g_t^{LDP}$ for a given dendron type is determined by the grafting density. It is anticipated that as $g$ approaches $g_t^{LDP}$, the LDP will tend to exhibit rigid-rod behaviour.[5]

In this work we study the structure of LDPs at thermodynamic equilibrium as a function of $g$ for relatively high grafting densities. The dendronisation of the backbone affects its conformation statistics and those of the dendra. Here we study these effects by looking at equilibrium average properties of the backbone and the dendra. The $g$-dependence of these properties is studied for model systems using Monte Carlo simulations of single LDPs in thermal equilibrium. Representative results are illustrated and discussed for a series of simple LDPs consisting of poly(*para*-phenylene) (PPP) backbone[6] with benzyl ether, Fréchet type dendrons[2,4,7] as shown in Scheme 1.

We chose to work with these systems both because of their nanoconductor applications interest[8] and because of computational advantages offered by their simple structure and the easily manageable number of internal degrees of freedom due to the nearly rigid phenyl ring units. The results obtained in this study apply to a single LDP in isolation, with main focus on the structure and mechanical properties, and are intended to be a first step in the development of suitable statistical thermodynamic tools for an efficient description of these massively flexible systems.

The remainder of the paper is organised as follows. The next

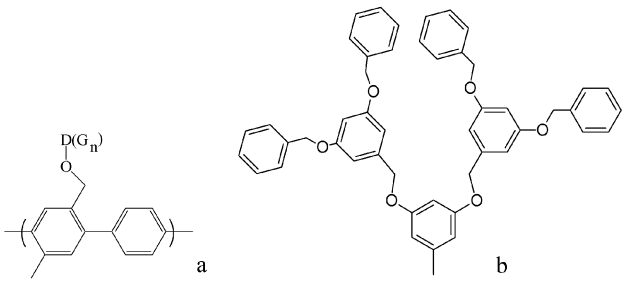


**Scheme 1** Poly(*para*-phenylene) (PPP) with benzyl ether, Fréchet type dendrons. Structures of (a) the repeat unit of the backbone polymer and (b) the dendritic unit (shown here with $g = 2$).

†Basis of a presentation given at Materials Discussion No. 6, 12–14th September 2003, Durham, UK.

 DOI: 10.1039/b304145j

section contains a description of the statistical measures employed to gain insights into the overall conformational properties of the LDP. This is followed by an account of the model used for the Monte Carlo studies and the parameterisation of that model. Next, the details pertaining to the Monte Carlo sampling techniques used to achieve equilibrium structures and to obtain a set of conformations that may be used for the statistical treatment are given. Then, we present the findings of these investigations and outline the implications of these results. Section 6 of the paper describes a phenomenological model that is consistent with the findings of this work and discusses the results in the context of this model. Finally, the conclusions are stated in section 7.

## 2. LDP conformation statistics

A simple LDP, of the generic structure shown in Scheme 1, consists of a linear backbone to which $N$ identical dendra are grafted at regularly spaced sites, labelled by $i = 1,2,...N$. Each dendron consists of $N_g$ segments labelled by the index $s = 1,2,...N_g$. A local frame of axes $x_i$, $y_i$, $z_i$ is attached to each grafting site (Fig. 1, inset a). The origin of this local frame defines the position, $\boldsymbol{R}_i$, of the site in a macroscopic common frame of reference $X$, $Y$, $Z$. The directions of the local frame axes $x_i$, $y_i$, $z_i$ define the orientation, $\omega_i$, of the site. The first site is taken to be fixed relative to the macroscopic frame. For simplicity, the internal structure of the backbone segments connecting two successive grafting sites is not considered explicitly in Fig. 1. The position of the $s$th segment of the $i$th dendron relative to the local frame is denoted by $\boldsymbol{r}_{s;i}$ (Fig. 1, inset b). Then, the conformational state, $n$, of such a supermolecule is fully specified given the positions, $\boldsymbol{R}_i$, of the grafting sites, their orientations, $\omega_i$, and the positions, $\boldsymbol{r}_{s;i}$, of all the segments of each dendron in its respective local frame. Accordingly, the conformation index, $n$, stands for the set of variables $\{R_i, \omega_i, r_{s;i}\}$.

Let $E(n)$ denote the internal (intra-molecular) energy of the $n$th conformational state of the LDP and $E'(n;q)$ denote the energy of interaction with its environment (be it a solvent, a substrate, a collection of other LDPs, *etc.*), the state of which is specified by the collective variable, $q$. Then the equilibrium probability, $p(n)$, for the LDP to be found in state $n$ is given by

$$p(n) = \sum_q \mathrm{e}^{-(E(n)+E'(n;q))/kT} \Big/ \sum_{n;q} \mathrm{e}^{-(E(n)+E'(n;q))/kT}. \qquad (1)$$

The equilibrium ensemble properties of the LDP can, in principle, be obtained by evaluating various moments of this probability distribution, *i.e.* averages, $\langle X \rangle$, of conformation dependent quantities, $X(n)$, obtained by sampling over all the accessible conformations according to

$$\langle X \rangle = \sum_n X(n)p(n). \qquad (2)$$

In the present study we consider two kinds of moments of the probability distribution, corresponding to the properties of the backbone and to the properties of the grafted dendra, as follows.

### Backbone properties

These include average distances between grafting sites, $\langle R_{i,j} \rangle = \langle |\boldsymbol{R}_i - \boldsymbol{R}_j| \rangle$, and higher moments, $\langle R^m_{i,j} \rangle$ ($m = 2, 3...$), of the relative spatial distribution of the grafting sites. Of particular interest is the average end-to-end distance of the backbone, $R_{\mathrm{e-e}} \equiv \langle R_{1,N} \rangle$, measuring the elongation of the LDP supermolecule, and the rms fluctuations $\sigma_{\mathrm{e-e}} \equiv \sqrt{\langle R^2_{1,N} \rangle - \langle R_{1,N} \rangle^2}$ of the end-to-end distance.

Averages associated with the relative orientations of the local axes frame of grafting site $i$ with respect to that of grafting site $j$ give information about the angular distribution of the dendra along the backbone. They also monitor the congestion-induced rigidity of the backbone with respect to bending and torsional motion. The local axis $z_i$ is taken along the *para*-axis of the phenyl at the $i$th grafting site, the $x_i$ axis is taken on the ring plane and the origin of the local frame is positioned at the ring centre (Fig. 1, inset a). Due to the statistical mirror symmetry of the grafted dendra, the ring plane at each grafting site is a local plane of symmetry.

Denoting collectively the unit vectors along the local axes of the $i$th site by $\boldsymbol{a}_i$, with $\boldsymbol{a} = \boldsymbol{x}, \boldsymbol{y}, \boldsymbol{z}$, and those of the $j$th site by $\boldsymbol{b}_j$ we may define the set of ensemble averages, $\langle \boldsymbol{a}_i \cdot \boldsymbol{b}_j \rangle$, describing the relative orientations of all pairs of grafting sites. The respective rms fluctuations, defined as

$$\sigma(a_i b_j) \equiv \sqrt{\langle (\boldsymbol{a}_i \cdot \boldsymbol{b}_j)^2 \rangle - \langle \boldsymbol{a}_i \cdot \boldsymbol{b}_j \rangle^2} \qquad (3)$$

provide a measure of the breadth of the distribution of the relative orientations of the local axes in sites $i$ and $j$. For unimodal distributions, the breadth defines the stiffness of the backbone with respect to internal reorientations of its segments. Therefore, $\sigma(a_i b_j)$ provides a measure of local stiffness through which the global mechanical response of the LDP can be evaluated.

### Dendron properties

These include averages associated with the position, $\boldsymbol{r}_{s;i}$, of the $s$th segment of the $i$th dendron. From the first rank averages, $\langle \boldsymbol{r}_{s;i} \rangle$, of all the segments of a dendron, its centre of mass,

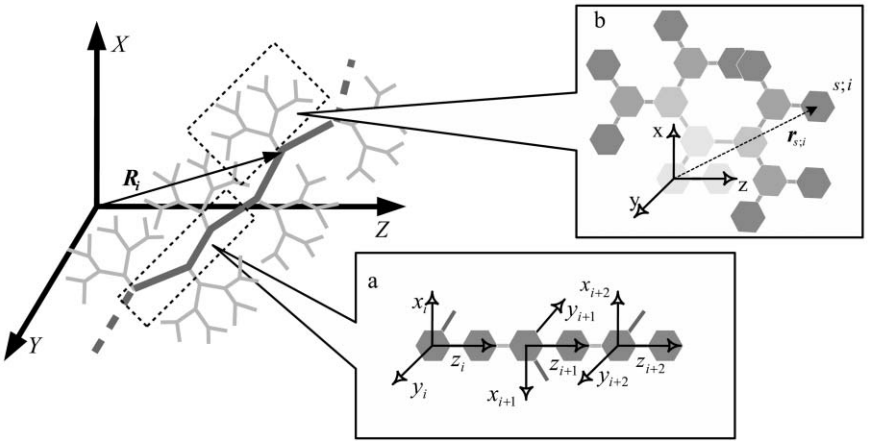


**Fig. 1** LDP topology and coordinates. Inset (a) local frame axes $x_i$, $y_i$, $z_i$ at grafting sites. Inset (b) position $\boldsymbol{r}_{s;i}$ of the $s$th dendron segment relative to the local frame.

$\boldsymbol{R}_{\mathrm{CM}}^{(i)}$, can be found in the local frame of the respective grafting site:

$$\boldsymbol{R}_{\mathrm{CM}}^{(i)} = \sum_s m_{s;i}\langle \boldsymbol{r}_{s;i}\rangle / \sum_s m_{s;i}\,, \tag{4}$$

where $m_{s;i}$ is the mass of the $s$th segment of the $i$th dendron.

From the second rank averages of the dendron segment positions, the moment of inertia tensor $I_{\mathrm{i}}^{\mathrm{ab}}$ of the mass distribution of the dendron can be determined in the local frame according to

$$\begin{aligned} I_i^{aa} &= \sum_s m_{s;i}\langle (\boldsymbol{a}\times\boldsymbol{r}_{s;i})^2\rangle \\ I_i^{ab} &= -\sum_s m_{s;i}\langle (\boldsymbol{a}\cdot\boldsymbol{r}_{s;i})(\boldsymbol{b}\cdot\boldsymbol{r}_{s;i})\rangle\,. \end{aligned} \tag{5}$$

The principal values of the inertia tensor provide quantification of the spatial extent and of the possible asymmetry of the mass distribution of the dendra.

In what follows we present calculations of the averages described above using the Metropolis Monte Carlo sampling method[9] for a model LDP consisting of repeat units (monomers) of the type shown in Scheme 1. In these calculations we neglect any conformation dependence of the interaction energy of the LDP with its surroundings, *i.e.* $E'$ of eqn. (1), and we make a number of simplifying assumptions in order to construct a coarse grained model for the intramolecular part of the energy $E(n)$. The details of this model are described in the next section.

## 3. Model description

The LDP supermolecule, consisting of a PPP backbone with benzyl ether Fréchet type dendra of specified generation (Scheme 1), is modelled at a level of detail which allows computational efficiency whilst maintaining the essential flexibility and intramolecular interactions of the system. On approaching steric congestion conditions the repulsive forces at short range become the dominant interactions within the supermolecule. Accordingly, we use, in a first approximation, a coarse-grained, excluded volume (athermal) description of the intra-molecular interactions. Our priority in extending the length and time scales in simulations of dendritic polymers is to coarsen the description of forces from all atoms to segments or to collections of atoms. To reduce the computational volume, the molecular system is partitioned into rigid bodies with constrained bond lengths. A rigid body (united atom) can consist either of a single atom (carbon or oxygen, belonging to single chemical bonds or methylene functional groups) or of a phenyl ring (either belonging to a dendron or to the backbone).

All bond lengths are fixed at standard values (in Å): C–$C_{ar}$ = 1.53, $C_{ar}$–$C_{ar}$ = 1.4 and C–O = 1.4. Phenyl rings, belonging to backbone or to dendra alike, are treated as regular hexagonal rigid structures with fixed bond lengths. Flexibility is introduced by allowing fluctuations of the bond angles for all the bonds in the structure, other than the bonds of the phenyl rings and, in addition, through bond torsion angles (rotations about single bonds). Each bond angle is taken to fluctuate freely by a maximum value $\delta_{\mathrm{bond}}$ about a fixed mean value $\vartheta_{\mathrm{bond}}^0$ corresponding to the minimum energy configuration of the respective bonds. The mean bond-angle values used are (O–C–C) = 112°, ($C_{ar}$–$C_{ar}$–C) = 120° and (C–O–C) = 109°. The required energy mapping was derived using commercial molecular mechanics (MM) software.[10] The angles, $\vartheta_{\mathrm{bond}}^0$ and $\delta_{\mathrm{bond}}$, used in our calculations, are within the range suggested by the MM software (Cerius2 program, assuming the Compass force field). In order to minimize the number of independent parameters of our simple model, the same value, $\delta_{\mathrm{bond}}$ = 20°, is ascribed to all bond angles. The torsion angles $\varphi$ of all bonds are completely unbiased to vary from 0° to 360°.

Hard body interactions are considered among phenyls or individual atoms (C or O). Accordingly, a spherical region around the centre of each united atom is excluded to any other united atom. In the present calculations the van der Waals radii of the hard spheres associated with the united atoms were set equal to 3.17 Å for the phenyl rings, 1.77 Å for methylene groups and 1.52 Å for oxygen atoms.

## 4. Monte Carlo sampling

For low dendron generations the initial LDP configuration is generated using equilibrium values for all bond angles and carefully chosen torsion angles to produce overlap-free structures. This scheme, however, becomes extremely inefficient for the fifth and higher generations due to space limitations. The same limitations, of course, underlie the difficulty in the chemical synthesis of the actual LDPs at high generations. The construction of a starting configuration in this case proceeds by initially using soft van der Waals spheres for all the united atoms of the dendra and progressively making the repulsions stronger, as more efficiently packed configurations are accessed, until a configuration can be realised with completely hard spheres. The soft repulsion between two overlapping van der Waals spheres in these preparatory runs was taken to be proportional to their overlap volume, $U = bV_{\mathrm{overlap}}^2$, with the positive coefficient $b$ increasing gradually. On reaching an overlap-free starting configuration, the LDP supermolecule is allowed to relax by successive MC steps to an equilibrium structure. The relaxation of the LDP, for each generation, from a number of different starting configurations to structures with common ensemble characteristics is indicative that equilibrium structures are obtained. Strictly, however, this does not ensure that the entire conformational phase space has indeed been sampled.

At each MC step, a bond angle or a torsion angle is chosen at random. These angles are then changed by amounts chosen randomly from an interval adjusted so that the acceptance rate for each type of move is approximately 0.35. Each new position of the rotated part of the molecule is checked for overlaps with the other parts of the molecule and is retained if the resulting configuration is overlap-free. The number of moves in a Monte Carlo cycle is, on average, equal to the number of degrees of freedom of each supermolecule. The number of MC cycles required for equilibration in these calculations typically ranges from $10^5$ MC cycles for small dendra (low $g$) to $10^6$ MC cycles for large dendra (high $g$). Upon reaching equilibration, various configurations of the systems are simulated by using the same move algorithms. A typical run consists of $10^6$ MC cycles. Structural data were collected every 10 MC cycles. The results and calculations were extracted from a set of conformations of the equilibrated system. This set consists of $10^4$ conformations for each supermolecule. MC simulations were performed on samples of single LDPs consisting of 10 repeat units (monomers) as well as on periodical LDPs, with a periodicity of 10 monomers, in order to avoid end effects.

## 5. Results and discussion

The average values of the end-to-end distance of the backbone as a function of generation and the respective rms deviations are shown in Fig. 2. For lower generations ($g$ = 1 to 3) the mean end-to-end distance shows no $g$-dependence. Noteworthy is the decrease of the end-to-end distance from $g$ = 4 to $g$ = 5. This is attributed to the development of congestion-generated twist and bend structures that cause the average relative disposition of consecutive backbone segments to deviate from linearity (see Fig. 3). This picture is supported by values of

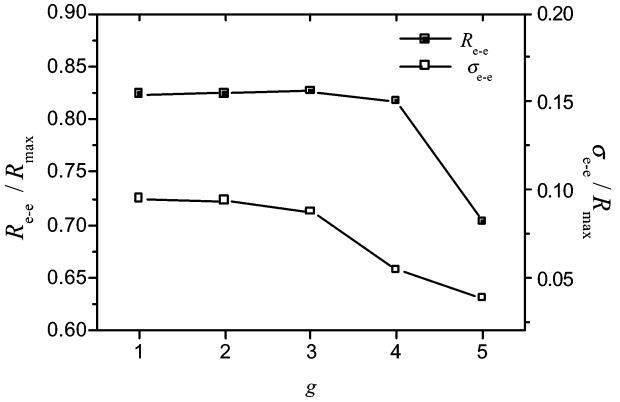


**Fig. 2** The reduced mean end-to-end distance, $R_{e-e}$, and the respective rms, $\sigma_{e-e}$, fluctuations as a function of dendron generation, $g$. $R_{max}$ denotes the length of the backbone at full extension.

segmental orientational averages to be described below. As is seen from the plot of $\sigma_{e-e}$ in Fig. 2, the rms fluctuations of the end-to-end distance decrease monotonously with $g$ as a result of the restrictions imposed on the conformations of the backbone by the increasing size of the grafted dendra.

Turning now to the ensemble averages that describe the relative orientations of the backbone segments, we note first that in the absence of any steric restrictions from the dendra all the $\langle \boldsymbol{a}_i \cdot \boldsymbol{b}_j \rangle$ ensemble averages should vanish except for the "torsion-independent" averages $\langle \boldsymbol{z}_i \cdot \boldsymbol{z}_j \rangle$. The vanishing of the other ensemble averages is a result of the free rotations assumed about the phenyl ring *para*-axes in conjunction with the symmetries of the repeat units and the choice of the local frame axes. The values of the $\langle \boldsymbol{z}_i \cdot \boldsymbol{z}_j \rangle$ averages, and of their respective rms fluctuations are dictated entirely by the unhindered sampling of all the relative orientations that are

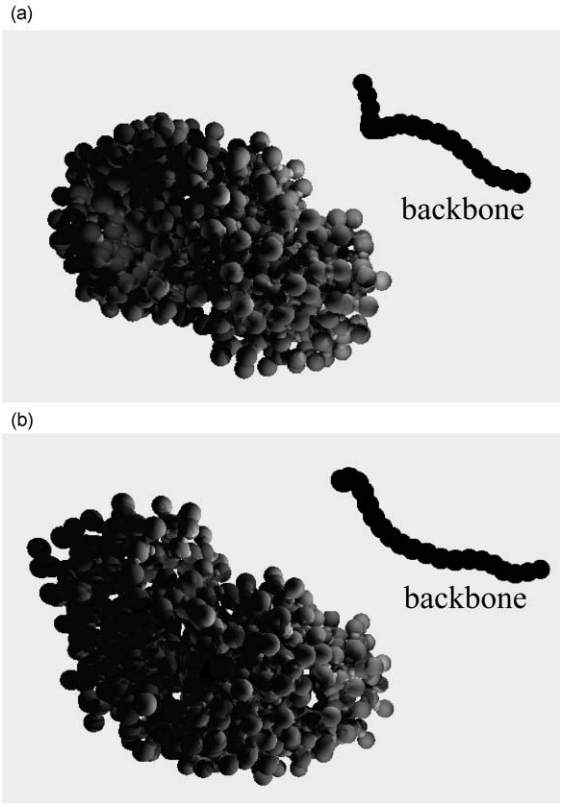


**Fig. 3** Snapshots illustrating two equilibrium structures of the 10-monomer LDP with $g = 5$ dendra attached. These two quasi-stable configurations are obtained from different starting configurations. Backbone conformations for each structure are inset for clarity.

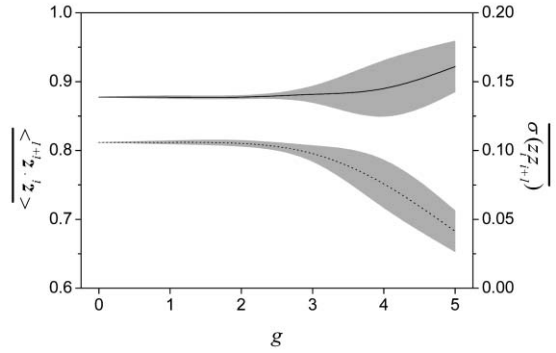


**Fig. 4** Mean values of $\overline{\langle \boldsymbol{z}_i \cdot \boldsymbol{z}_{i+1} \rangle}$ (solid line) and of the corresponding rms fluctuations $\overline{\sigma(z_i z_{i+1})}$ (dotted line), as a function of dendron generation. The shaded areas represent the magnitude of the spread of these quantities about their mean values according to eqn. (8).

consistent with the limiting angle $\delta_{bond} = 20^\circ$ between the *para*-axes of successive phenyl rings along the contour from site $i$ to site $j$. The same considerations apply to the rms fluctuations associated with the ensemble averages involving the transverse local axes $x_i$, $y_i$. The general behaviour of the local orientational ensemble averages remains essentially unchanged for $g = 0$ to 3 (see Fig. 4–6), except that some signs of dendron size effects become detectable on the averages $\langle \boldsymbol{x}_i \cdot \boldsymbol{x}_{i+1} \rangle$. The latter acquire small but negative values, indicating a slight preference of the antiparallel pairing of first neighbour dendra so as to maximise their mutual distance. The same preference towards distance maximizing configurations is reflected on the positive values acquired by $\langle \boldsymbol{z}_i \cdot \boldsymbol{x}_{i+1} \rangle$ in Fig. 5. A slight decrease in the rms fluctuations associated with these averages is observed, in accordance with the appearance of some constraints on the relative orientations of backbone segments as the size of the dendra increases. Furthermore, the calculated values of all the ensemble averages $\langle \boldsymbol{a}_i \cdot \boldsymbol{b}_{i+1} \rangle$ are, aside from end effects, independent of the site index $i$, indicating that the equilibrium sampling of orientations is the same in all the grafting sites. In summary, the low generation averages ($g = 0$ to 3) show little effect of the dendronisation on the backbone, they show large values of rms fluctuations but are sharply defined, *i.e.* with negligible spread ($i$-dependence) on going from one site to the other.

The picture changes qualitatively above $g = 3$. The ensemble averages for $g = 4$, and more so for $g = 5$, show strong effects of dendronisation. First, the fluctuations about the average values decrease substantially, in accordance with the expected narrowing of the orientational distributions due to dendron mass crowding in the periphery of the backbone. More importantly, however, the calculated ensemble averages show considerable dependence on the site index $i$, indicating the

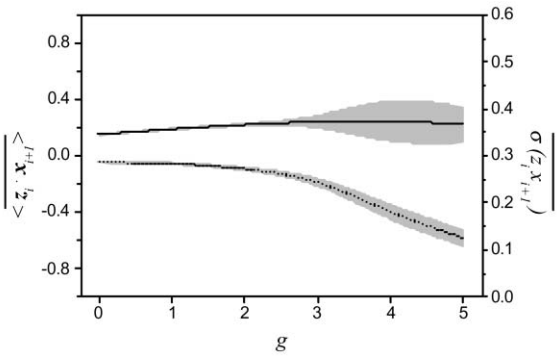


**Fig. 5** Mean values of $\overline{\langle \boldsymbol{z}_i \cdot \boldsymbol{x}_{i+1} \rangle}$ (solid line) and of the corresponding rms fluctuations $\overline{\sigma(z_i x_{i+1})}$ (dotted line), as a function of dendron generation. The shaded areas represent the magnitude of the spread of these quantities about their mean values according to eqn. (8).

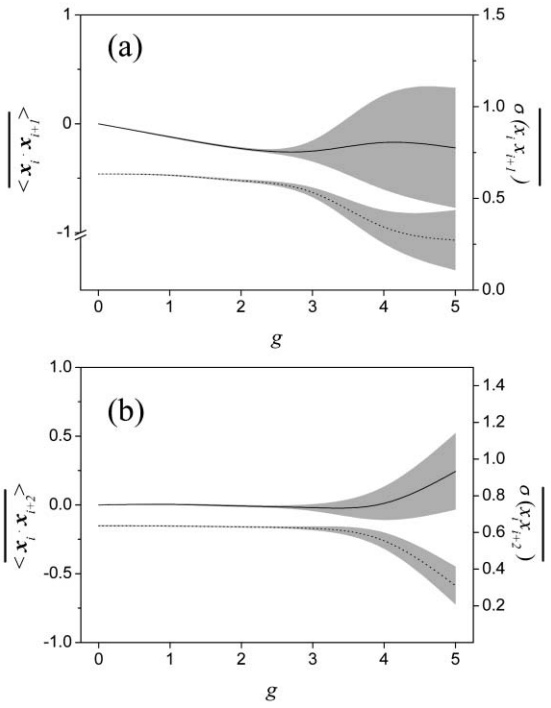


**Fig. 6** Mean values of a) $\overline{\langle \boldsymbol{x}_i \cdot \boldsymbol{x}_{i+1} \rangle}$ and b) $\overline{\langle \boldsymbol{x}_i \cdot \boldsymbol{x}_{i+2} \rangle}$ (solid lines) and of their respective rms fluctuations, $\sigma(x_i x_{i+1})$ and $\sigma(x_i x_{i+2})$ (dotted lines), as a function of dendron generation. The shaded areas represent the magnitude of the spread of these quantities about their mean values according to eqn. (8).

presence of structures that break the full symmetry of translation along the backbone contour. These structures are attributed to the entrapment of the high generation LDP into different long-lived, quasi-stable configurations that, because of peripheral crowding, do not convert with one another easily. The snapshots of two such configurations, obtained from different starting conditions of the simulation, are shown in Fig. 3.

The *i*-dependence of the evaluated ensemble averages does not show any clear regularity over the contour scale of the present simulations (10 repeat units of the LDP). Accordingly, the results of the calculations of the orientational ensemble averages are reported as mean values over the various sites *i*. The mean value of a site-dependent ensemble average $\langle X_i \rangle$ over $N'$ consecutive sites is denoted by

$$\overline{\langle X_i \rangle} \equiv \sum_{i=i'}^{i'+N'-1} \langle X_i \rangle / N' . \qquad (6)$$

A measure of the spread $\Delta\overline{\langle X_i \rangle}$ of the ensemble averages $\langle X_i \rangle$ about their mean value $\overline{\langle X_i \rangle}$ is provided by the standard deviation, namely

$$\Delta\overline{\langle X_i \rangle} \equiv \sqrt{\overline{\langle X_i \rangle^2} - \left(\overline{\langle X_i \rangle}\right)^2} . \qquad (7)$$

Fig. 4 shows the mean values of the ensemble averages of the $\langle \boldsymbol{z}_i \cdot \boldsymbol{z}_{i+1} \rangle$, together with the spread about the mean values, as a function of dendron generation. The corresponding rms fluctuations $\sigma(z_i z_{i+1})$ also show some site dependence with increasing *g*. Accordingly, the mean values of these fluctuations and the respective spreads have been determined. These are also shown in Fig. 4. The mean values and spreads are calculated according to eqn. (6) and (7), respectively, using $i' = 3$ and $N' = 6$

It is apparent from these plots that up to $g = 3$, $\overline{\langle \boldsymbol{z}_i \cdot \boldsymbol{z}_{i+1} \rangle}$ and $\overline{\sigma(z_i z_{i+1})}$ maintain essentially the values corresponding to unhindered sampling of the relative orientations of the $\boldsymbol{z}_i$, $\boldsymbol{z}_{i+1}$ axes and show negligible spread along the backbone contour. Above $g = 3$, the spread of both quantities increases rapidly. At $g = 5$, the rms fluctuations $\sigma(z_i z_{i+1})$ are rather limited while the mean value of $\langle \boldsymbol{z}_i \cdot \boldsymbol{z}_{i+1} \rangle$ shows a clear increase. This increase, however, does not result from a stronger tendency towards co-linearity of the $\boldsymbol{z}_i$, $\boldsymbol{z}_{i+1}$ axes. As suggested by the small mean value of $\overline{\sigma(z_i z_{i+1})}$ at $g = 5$, the two axes assume on the average slightly bent (by 10–20°) configurations relative to one another and have limited freedom to fluctuate about these configurations.

The locally bent backbone picture is supported by the results of the calculations of the ensemble averages $\overline{\langle \boldsymbol{z}_i \cdot \boldsymbol{x}_{i+1} \rangle}$. Their mean values, together with the mean values of their rms fluctuations and the respective spreads, are plotted in Fig. 5 as a function of *g*. These plots exhibit the same general trends as those of Fig. 4, namely, decreasing rms fluctuations and increasing spread with increasing *g*. Moreover, it is clear from the $\overline{\langle \boldsymbol{z}_i \cdot \boldsymbol{x}_{i+1} \rangle}$ plot that at $g = 5$ the $x_{i+1}$ axis maintains a considerable positive projection along the $z_i$ axis, indicating a systematic bias towards bent configurations. The sense of bending is singled out by the symmetry breaking with respect to the local $(yz)_i$ plane resulting from the attachment of the dendra in the positive direction of the $x_i$ axis. On the other hand, the grafted dendra, when not interacting with their neighbours, grow symmetrically, in a statistical sense, with respect to the $(xz)_i$ plane and furthermore the interactions among the dendra are mirror-symmetric. Accordingly, the ensemble averages $\langle \boldsymbol{y}_i \cdot \boldsymbol{z}_{i+1} \rangle$ should vanish by symmetry. The calculations show that this holds locally (*i.e.* for each grafting site *i*) only for $g \leqslant 3$ while for higher generations only the mean values, $\overline{\langle \boldsymbol{y}_i \cdot \boldsymbol{z}_{i+1} \rangle}$, vanish and there is considerable spread (reaching $\pm 0.3$ for $g = 5$) of $\langle \boldsymbol{y}_i \cdot \boldsymbol{z}_{i+1} \rangle$ over individual sites. This local breaking of mirror symmetry, and its simultaneous validity on a global scale, is an additional manifestation of the quasi-stability of curled configurations resulting from the strong dendritic crowding around the backbone. The form of the curling is irregular, at least on the length scale of the 10 monomer sample. However, it is expected that the introduction of a chiral perturbation into the dendron structure would favour the persistence of uniform curling along the backbone contour thus generating a helical LDP of well defined average pitch.

The results of the calculations of the ensemble averages $\langle \boldsymbol{x}_i \cdot \boldsymbol{x}_{i+1} \rangle$ are plotted in Fig. 6a. Here, in addition to the general trend of decreasing fluctuations and increasing spread with *g*, it is apparent that a slight preference towards antiparallel configurations of consecutive $x_i$ axes is maintained for all generations. However, the large spread at $g = 5$ indicates that this preference is opposed at some sites by the formation of the local quasi-stable asymmetric structures discussed earlier. Finally, the results on $\overline{\langle \boldsymbol{x}_i \cdot \boldsymbol{x}_{i+2} \rangle}$, plotted in Fig. 6b, show that up to $g = 4$ the correlations between the transverse axes of second-neighbour sites are negligible. At $g = 5$ there is a tendency towards parallel configurations, in accord with the antiparallel preference shown by nearest neighbours. The relatively large value of the rms fluctuations persisting at $g = 5$ suggest that the peripheral crowding does not restrict the twisting of the backbone very strongly. In making inferences from the results shown in Fig. 6 it should be kept in mind that although the $\langle \boldsymbol{x}_i \cdot \boldsymbol{x}_{i+1} \rangle$ and $\langle \boldsymbol{x}_i \cdot \boldsymbol{x}_{i+2} \rangle$ averages reflect primarily the torsional behaviour of the backbone, they are also influenced by the local bending to an extent controlled by the angle $\delta_{\text{bond}}$ allowed for the consecutive ring *para*-axes along the backbone contour.

The implications of packing on the ensemble-average structure of the grafted dendra are presented in Fig. 7 by means of the average mass distribution of a single dendron with respect to the "dendron centre", namely the centre of the innermost phenyl ring ($g = 0$ ring) of the dendron (local frame shown in inset (b) of Fig. 1). Fig. 7a shows, for $g = 3$, the average (over dendron conformations and for dendra at different grafting sites) mass density $\bar{\eta}(r)$ as a function of

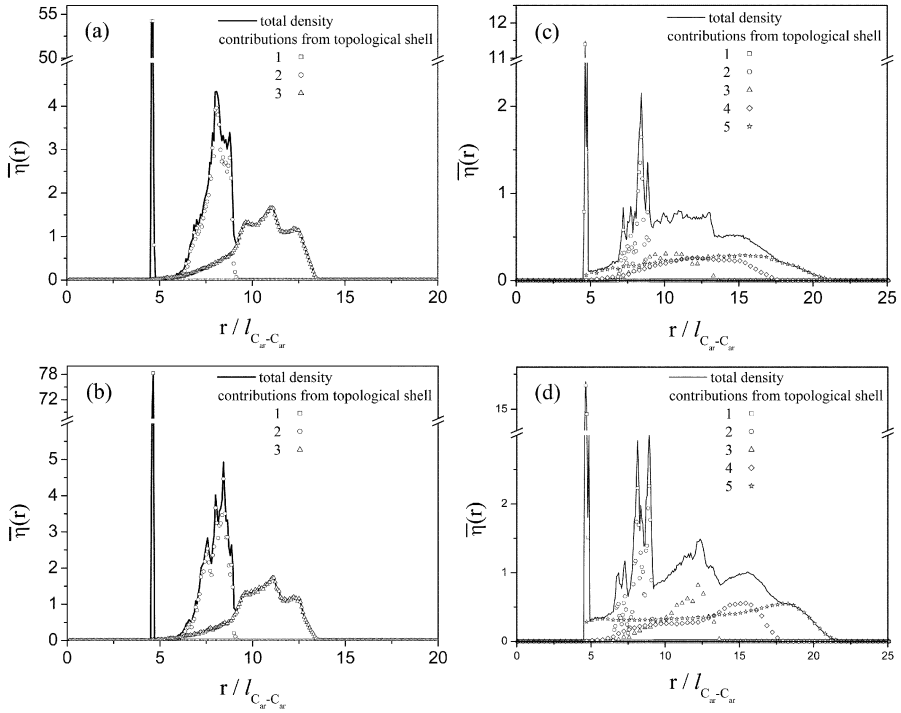


**Fig. 7** Density profiles of a) the $g = 3$ LDP, b) a $g = 3$ monomeric dendron, c) the $g = 5$ LDP and d) a $g = 5$ monomeric dendron. Each profile shows the average mass distribution, $\bar{\eta}(r)$ as a function of the distance from the dendron centre $r$, in units of the $C_{ar}$–$C_{ar}$ bond length (1.4 Å), and the breakdown of the profile into the contributions from each topological shell corresponding to each successive generation.

distance $r$ from the dendron origin, expressed in units of the length $l_{C_{ar}\text{–}C_{ar}}$ of the $C_{ar}$–$C_{ar}$ bond (1.4 Å). The density is obtained by calculating the dendritic mass that is contained within a thin spherical shell of radius $r$, *i.e.* $\bar{\eta}(r)$ represents an average density profile over all directions. The total density distribution as well as the separate contributions from the groups of atoms belonging to the first, second and third topological shell of the $g = 3$ dendron are shown. The sharp peaks seen at approximately $r = 4.64$ correspond to the first topological shell, where little positional variation is possible. It is apparent that there is some penetration of segments of the third (outer) shell into the region of the second and possibly the first shell. Fig. 7b shows the same density profiles only for a free dendron (*i.e.* not attached to the backbone). Here we see little change in the profile between a free dendron and dendra that are attached to the polymer. However, we see in Fig. 7c and d, which show the same profiles for $g = 5$, that the distribution of the outer topological shells of the larger dendra changes substantially on attachment to a linear chain. The density profile in Fig. 7c indicates that segments of the fifth (outermost) topological shell penetrate considerably into the regions of inner shells. However, this is due only in part to backfolding of the dendritic branches, as has been observed previously,[11,12] being significantly influenced by the spatial expansion of a single dendron to the extent that it can locally wrap itself around the backbone. This effect is consistent with the calculations of the centre of mass position, to be discussed below. Comparison with the profile of the free dendron in Fig. 7d shows considerable deformation of the mass distribution as a result of the constraints imposed on the grafted dendron by its surroundings. Among the general characteristics of the diagrams in Fig. 7 are (i) that the peaks associated with the different topological shells can be more or less clearly identified on the total density profile, (ii) that these peaks become broader on moving to the outer (third, fourth and fifth) shells as a result of the smearing of the mass distribution of these shells and (iii) that, aside from the peaks, the density profile shows an overall decreasing trend from the centre of the dendron to its periphery.[13–19]

The global features of the dendron mass distribution, as a function of generation, are described by means of the position of the dendron centre of mass in the local frame, presented in Fig. 8, and by means of the dendron moments of inertia in their principal axis frame, shown in Fig. 9.

It is worth noting in Fig. 8 that for high dendron generations the mean position of the centre tends towards the local $x$-axis, as indicated by the decrease of the magnitude of the $Z_{CM}$ component, and that the mean distance $\bar{R}_{CM}$ of the centre of mass from the origin of the grafting site local frame increases in comparison with the monomer. This indicates that the monomer is able to expand in all directions, but, the grafted dendra are unable to grow in the direction along the backbone due to the neighbouring dendra sites. These calculations also indicate that a considerable part of the dendron mass is distributed opposite to the grafting side of the backbone. In other words, the $g = 5$ dendra are wrapped around the backbone.

The mean values of the principal moments of inertia, $\bar{\boldsymbol{I}}_{xx}$, $\bar{\boldsymbol{I}}_{yy}$ and $\bar{\boldsymbol{I}}_{zz}$, of the dendra describe the overall shape of the grafted dendra. From these moments of inertia, given in Fig. 9a, it is evident that with increasing dendron generation $\bar{\boldsymbol{I}}_{yy}$ and $\bar{\boldsymbol{I}}_{zz}$ become progressively different. This difference is consistent with an overall shape change from a prolate ellipsoid to an asymmetric spheroid. As expected from the symmetry of the LDP, the mean direction of the principal $y$-axis of the moment of inertia tensor coincides with the $y$-axis of the local frame. Accordingly the change of direction of the principal axes of inertia relative to the local frame can be fully represented by $\boldsymbol{x}\cdot\boldsymbol{Z}_p$, shown in Fig. 9b, where $\boldsymbol{x}$ is the $x$-axis in the local frame and $\boldsymbol{Z}_p$ is the $z$-axis of the principal frame. The variation of $\boldsymbol{x}\cdot\boldsymbol{Z}_p$ with $g$ indicates that in order to pack efficiently at intermediate $g$, the dendra adopt a configuration where they tilt towards the backbone, whereas at high $g$ the second neighbour interaction causes the dendra to shift back towards an average configuration that puts the principal frame closer to the local frame. These effects are discussed further in relation to a phenomenological model in the section that follows.

In order to compare the average size of the dendra with the

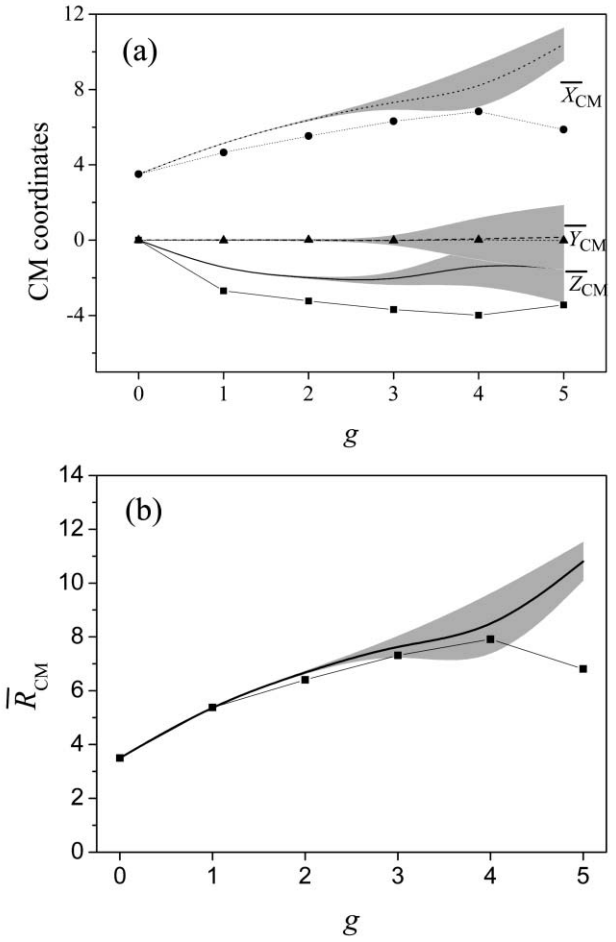


**Fig. 8** (a) The components of the centre of mass of the dendron in the local frame with data points plotted as filled circles, triangles and squares to represent the monomer values of the $\bar{X}_{CM}$, $\bar{Y}_{CM}$ and $\bar{Z}_{CM}$ components respectively. (b) The distance of the centre of mass from the local frame origin plotted as a function of dendrimer generation, $g$. The data points represented by squares show the monomer values for each generation. In both plots, shaded regions represent the spread of the data for the polymer. The length scales in both graphs are in units of the $C_{ar}$–$C_{ar}$ bond length (1.4 Å).

spacing between grafted sites, the moments of inertia have been used to calculate an average dendron radius (*i.e.* the radius of a sphere whose moment of inertia is equal to the average of the principal moments of the dendron). This radius,

$$R_d = \frac{(I_{xx} + I_{yy} + I_{zz})^{1/2}}{(6m/5)^{1/2}}, \quad (8)$$

where $m$ is the mass of the dendra, is plotted in Fig. 10 as a function of dendron generation. Here we see that for all dendra generations with $g > 0$ the mean dendron radius, $R_d$, is greater than the distance $L$ between grafting sites, indicating that overlap between neighbouring dendra on the LDP is possible at low generations and that the extent of overlapping is intensified with increasing $g$.

## 6. A phenomenological model

In this section we incorporate the essential findings of the simulations into a phenomenological model of the LDP in terms of effective interactions among its constituent repeat units. We start out by picturing the LPD as a chain of completely rigid repeat units $i = 1,2...N$ taken to consist of linearly linked segments of length $L$, to which spherical blobs of diameter $D$, representing the dendra, are laterally attached. The direction of a linear segment is identified with the local $z_i$ axis and the centre of the spherical blob is taken for simplicity to lie on the $x_i$ axis, a distance, $h$, from the origin (see Fig. 11a). Both $D$ and $h$ depend on dendritic generation, $g$.

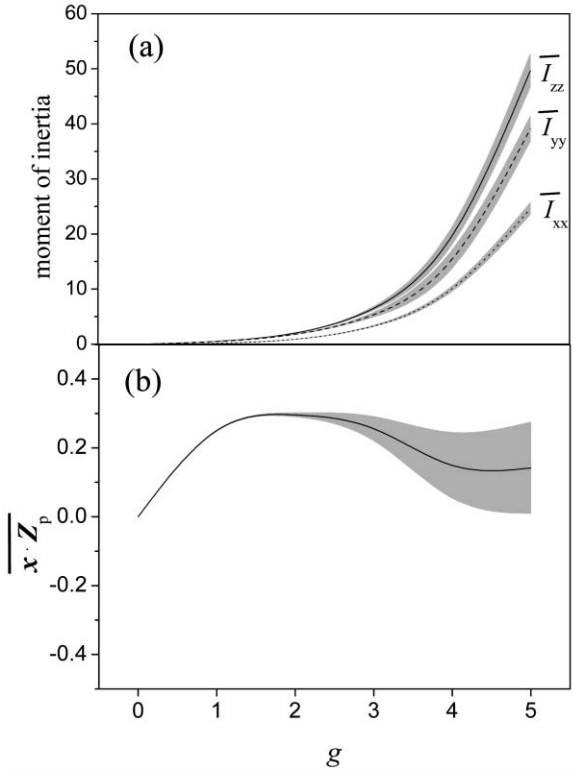


**Fig. 9** (a) The principal moments of inertia, $\bar{I}_{xx}$, $\bar{I}_{yy}$ and $\bar{I}_{zz}$, in units of $m_{ph}\cdot(l_{C_{ar}}–C_{ar})^2$, where $m_{ph}$ is the phenyl ring mass, and (b) the projection of the local frame $x$-axis relative to the principal $z$-axis of the LDP as a function of the dendra generation, $g$. Shaded regions represent the spread of this data over dendron grafting sites.

The results of the previous section suggest that as the generation increases, the global properties of the chain change qualitatively as follows:

(i) The average elongation of the chain decreases while its elastic modulus increases. In a Gaussian coil approximation for the chain the elastic modulus is inversely proportional to the rms fluctuations of the end-to-end distance.[20] Accordingly, the results in Fig. 2 would suggest that the linear elastic modulus of the LDP at $g = 5$ increases by a factor of 2.4 relative to the $g = 0$ value while the elongation shrinks by 15%.

(ii) The bending modulus of the LDP increases. Within the Gaussian approximation again, the bending modulus is inversely proportional to the linkage angle rms fluctuations, which, for small angles, are given by $1 - \overline{\langle z_i \cdot z_{i+1} \rangle}$. According

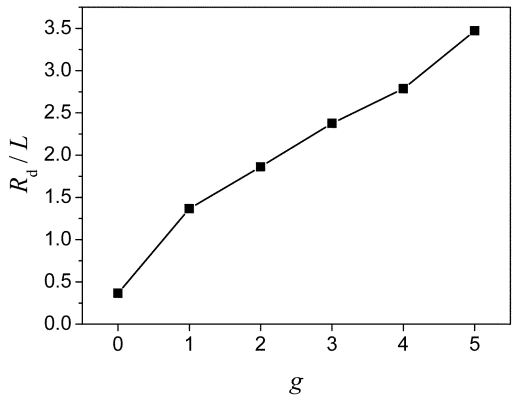


**Fig. 10** Calculated effective radius, $R_d$, of the grafted dendra, in units of the grafting distance, $L$, as a function of generation, $g$.

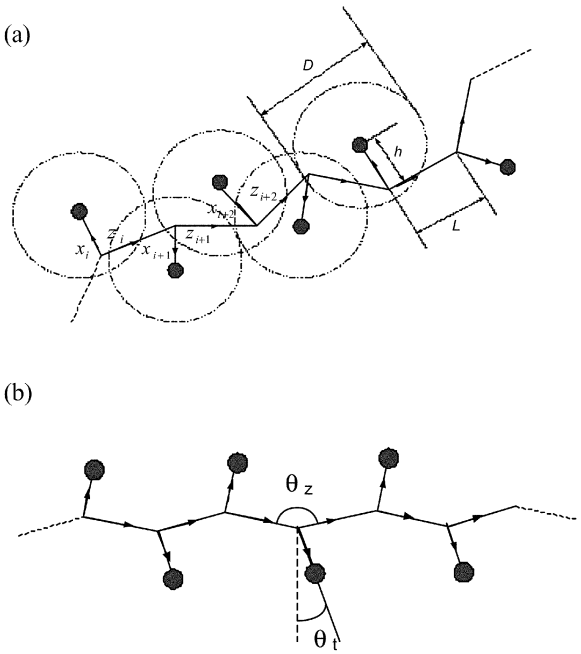


**Fig. 11** Schematic diagrams representing (a) the geometry of the phenomenological model, where $L$, $D$ and $h$ denote the segment length, "blob" diameter and distance of the "blob" centre to the polymer backbone respectively, and (b) the minimum energy conformation resulting from the nearest neighbour interactions in eqn. (11), showing the "zig-zag angle", $\theta_z$, of the backbone segments and the dendra tilt angle, $\theta_t$, with respect to the backbone contour.

to Fig. 4 this suggests that dendronisation at $g = 5$ induces an increase of the bending modulus by a factor of 1.5 relative to $g = 0$.

These trends are, of course, not mutually independent; their common origin is traced back to the restrictions imposed on relative reorientations of the chain by the presence of the dendra. Furthermore the evaluation of the elastic constants from rms fluctuations within the Gaussian approximation is meaningful only for small deformations around the average state of the LDP, thus precluding the description of non-linear response. A more detailed consideration of the interactions among the repeat units of the LDP is therefore necessary in order to rationalize and unify the different aspects of its behaviour as a function of dendritic generation.

To this end we write the phenomenological conformational energy, $H$, of the LDP chain as a sum, $H = H_0 + H_D$, of a "bare" backbone term, $H_0$, and a term, $H_D$, associated with the interactions originating from the attachment of the dendra to the repeat units. The $H_0$ term is assumed to favour the mutual alignment of the consecutive repeat segments of the backbone, with the perfectly aligned conformation corresponding to the energy minimum, and also to inhibit large bending angles and self-intersecting conformations of the backbone. The $H_D$ term is assumed to depend on the distances $d_{i,j}$ between the centres of the dendritic blobs in sites $i$ and $j$, with distant pairs (*i.e.* parts for which $d_{i,j}$ is large compared to the effective diameter of the dendritic blob) contributing negligibly. Accordingly, $H_D$ can be written as a sum of nearest neighbour terms $H^{(1)}(d_{i,i+1})$, second neighbour terms $H^{(2)}(d_{i,i+2})$, *etc*, namely,

$$H_D = \sum_{i=1}^{N-1} H^{(1)}(d_{i,i+1}) + \sum_{i=1}^{N-2} H^{(2)}(d_{i,i+2}) + \ldots \qquad (9)$$

The detailed dependence of the $H^{(1)}$, $H^{(2)}$ terms on $d_{i,j}$ is not crucial. However, it is expected that these terms are essentially repulsive, tending to maximize the inter-blob distances, and that they would become negligible if the blob diameter $D$ became substantially smaller than the distance of closest approach of the blob centres, which is determined by the backbone flexibility. Thus on lowering the generation $g$, the reduction of the diameter $D$ should annihilate first the $H^{(2)}$ terms and further the $H^{(1)}$ terms. A very crude representation of these requirements is provided by the forms

$$H^{(1)}(d_{i,i+1}) = -vd_{i,i+1}^2 \qquad (9\ )$$

and

$$H^{(2)}(d_{i,i+2}) = -v'd_{i,i+2}^2 \qquad (10)$$

*i.e.* by taking the interactions to be proportional to the square of the blob distance, with $v'$ and $v$ vanishing when $D$ is substantially smaller than $2L$ and $L$ respectively. In this case the nearest neighbour interaction terms are, to within a trivial constant,

$$H^{(1)}(d_{i,i+1}) = -2vh(\boldsymbol{z}_i\cdot\boldsymbol{x}_{i+1} - h\boldsymbol{x}_i\cdot\boldsymbol{x}_{i+1}), \qquad (11)$$

with all distances expressed in units of $L$. This interaction form favours the alternating disposition of successive blob centres with respect to the backbone (antiparallel configuration of successive local $x$-axes) and a tilt of the $x$-axis of each site towards the positive $z$ direction of the preceding repeat unit. It leads to a minimum energy conformation as shown in Fig. 11b, *i.e.* with a planar zig-zag disposition of the backbone and an alternating configuration of the blobs on the same plane, with the local $x$-axes tilted relative to the mean backbone axis. The zig-zag angle, $\theta_z$, and the associated blob tilt angle, $\theta_t$, depends on the intrinsic stiffness of the backbone, *i.e.* the $H_0$ part, but increases with decreasing $h$. This minimum energy conformation explains the overall decrease of the elongation and the simultaneous decrease of its fluctuations at large dendron generation, as observed in Fig. 2. It also accounts correctly for the trends of $\overline{\langle \boldsymbol{z}_i\cdot\boldsymbol{x}_{i+1}\rangle}$ and $\overline{\langle \boldsymbol{x}_i\cdot\boldsymbol{x}_{i+1}\rangle}$ observed in Fig. 5 and 6 respectively.

The second neighbour terms of eqn. (10) have the following angular dependence

$$H^{(2)}(d_{i,i+2}) = -2v'(\boldsymbol{z}_i\cdot\boldsymbol{z}_{i+1} + h\boldsymbol{z}_i\cdot\boldsymbol{x}_{i+2} + h\boldsymbol{z}_{i+1}\cdot\boldsymbol{x}_{i+2} - h\boldsymbol{z}_{i+1}\cdot\boldsymbol{x}_i - h^2\boldsymbol{x}_i\cdot\boldsymbol{x}_{i+2}). \qquad (12)$$

It is evident that some of the terms in the right hand side of this equation counteract the minimum energy conformation favoured by the nearest neighbour interactions of eqn. (11). In particular, the first term in eqn. (12) favours the alignment of successive $z$-axes, thus opposing the backbone zig-zag pattern. More importantly, the last term favours antiparallel configurations of the $x$-axes of second neighbour segments and this of course cannot occur simultaneously with the antiparallel configurations of first neighbours, favoured by eqn. (11). This frustrated competition between first and second neighbour interactions leads to minimum energy conformations that are non-planar, although each of the individual contributions has a plane of symmetry. This escape to non-planarity accounts for the observed backbone configurations shown in Fig. 3 and for the observation of non-vanishing, albeit symmetrically spread about zero, values of $\langle \boldsymbol{z}_i\cdot\boldsymbol{y}_{i+1}\rangle$.

It is worthy of note that the energy associated with rotation around the polymer backbone and subsequent steric forces arising from interactions of neighbouring dendra will not be stored as the torsional rotation increases beyond a full turn. Thus, this energetic component has the form of a periodic torsional potential rather that a twist elastic energy.

It is apparent from the above considerations that the simple phenomenological model of eqn. (9) to (12) readily accounts for the MC simulation results regarding the behaviour of the backbone as a function of dendron generation $g$. The latter enters into the model through the parameters $v$, $v'$ and $h$ which,

by their definition, depend on the size and centre of mass position of the dendra. However, it should be noted that, at this level of the phenomenology, the deformability of the dendra is not taken into account and therefore correlations between the shape of the dendra and their relative distance from their neighbours are not dealt with. A complete phenomenological description of the LDP should, of course, provide a self-consistent explanation for the behaviour of both the backbone and the dendra. The simulated behaviour of the dendron mass distribution provides useful ingredients for the development of such a description. However, such development is beyond the scope of this work.

## 7. Conclusions

In this work, we have investigated the conformational behaviour of a poly(*para*-phenylene) LDP by Monte Carlo simulation, using hard-body repulsion to represent the intramolecular interactions. The shapes and relative orientations of neighbouring dendra as well as the induced stiffness and local structure of the backbone have been calculated for polymers functionalised with generation 1–5 dendra. A phenomenological model has been proposed that is consistent with these results. We find that for lower generations, $g \leqslant 3$, the LDP conformations are essentially unhindered and therefore the chain retains flexibility. At the fourth generation the relative orientation of the monomers become more restricted due to the increasing steric effects of the dendra. However, it is not until $g = 5$ that we see a definite change in the configuration and a local symmetry breaking associated with the type of congestion that leads to nearly rigid conformations. In this extremely crowded supermolecule it is necessary for the backbone to become engulfed in order for the dendra to access the requisite packing volume. In these calculations, the polymer begins to curl at this level of crowding, leading to the contraction of the end-to-end distance.

## Acknowledgements

D. K. C. and D. J. P. would like to thank Prof. Dieter Schlüter for stimulating discussions. This work is supported by the Caratheodore program of the University of Patras. Support from the RTN Project "Supermolecular Liquid Crystal Dendrimers – LCDD" (HPRN-CT2000-00016) is also acknowledged.

## References

1 G. R. Newkome, C. N. Moorefield and F. Vögtle, *Dendritic Molecules. Concepts, Syntheses, Perspectives*, VCH, Weinheim, Germany, 1996.
2 J. M. Fréchet and C. J. Hawker, in *Comprehensive Polymer Science, 2nd suppl.*, ed. S. Aggarwal and S. Russo, Pergamon Press, Oxford, UK, 1996, pp. 234–298.
3 A. W. Bosman, H. M. Janssen and E. W. Meijer, *Chem. Rev.*, 1999, **99**, 1665.
4 A. D. Schlüter and J. P. Rabe, *Angew. Chem., Int. Ed.*, 2000, **39**, 864.
5 N. Ouali, S. Mery and A. Skoulios, *Macromolecules*, 2000, **33**, 6185.
6 A. J. Berresheim, M. Muller and K. Mullen, *Chem. Rev.*, 1999, **99**, 1747.
7 J. M. Fréchet, C. J. Hawker, I. Gitsov and J. W. Leon, *J. Macromol. Sci., Part A: Pure Appl. Chem.*, 1996, **33**, 1399.
8 P. Kovacic and M. B. Jones, *Chem. Rev.*, 1987, **87**, 357.
9 M. Allen and D. Tildesley, *Computer Simulation of Liquids*, Oxford University Press, Oxford, UK, 1989.
10 Cerius$^2$ v.4.1, Molecular Modelling Software, available from Accelrys Ltd., 230/250 The Quorum, Barnwell Road, Cambridge CB5 8RE, UK (www.accelrys.com).
11 R. Klopsch, P. Franke and A. D. Schlüter, *Chem. Eur. J.*, 1996, **2**, 1330.
12 B. Karakaya, W. Claussen, K. Gessler, W. Seanger and A. D. Schlüter, *J. Am. Chem. Soc.*, 1997, **119**, 3296.
13 P. G. deGennes and H. J. Hervet, *Phys. Lett. Fr.*, 1983, **44**, L351.
14 M. L. Mansfield and L. I. Klushin, *Macromolecules*, 1993, **26**, 4262.
15 M. Murat and G. S. Grest, *Macromolecules*, 1996, **29**, 1278.
16 D. Boris and M. Rubinstein, *Macromolecules*, 1996, **29**, 7251.
17 K. Karatasos, D. B. Adolf and G. R. Davies, *J. Phys. Chem.*, 2001, **115**, 5310.
18 N. Zacharopoulos and I. G. Economou, *Macromolecules*, 2002, **35**, 1814.
19 H. M. Harreis, C. N. Likos and M. J. Ballauf, *J. Chem. Phys.*, 2003, **118**, 1979.
20 A. Y. Grosberg and A. R. Khoklov, *Statistical physics of macromolecules*, AIP Press, New York, 1994.